

Second Harmonic Generation Imaging Distinguishes Both High-Grade Dysplasia and Cancer from Normal Colonic Mucosa

John W. Birk · Micheal Tadros · Koorosh Moezardalan ·
Oleg Nadyarnykh · Faripour Forouhar ·
Joseph Anderson · Paul Campagnola

Received: 21 October 2013 / Accepted: 17 March 2014 / Published online: 18 April 2014
© Springer Science+Business Media New York 2014

Abstract

Background and Aim Second harmonic generation (SHG) is a novel imaging technology that could provide optical biopsy during endoscopy with advantages over current technology. SHG has the unique ability to evaluate the amount of extracellular matrix collagen protein and its alignment.

Methods Hematoxylin- and eosin-stained slides from colon biopsies (normal, low-grade dysplasia (LGD), high-grade dysplasia (HGD), and cancer) were examined with SHG imaging. Both signal intensity and collagen fiber alignment were measured. Average intensity per pixel (AIPP) was obtained, and an analyzing polarizer was used to calculate β , an alignment parameter.

Results The mean AIPP for normal mucosa was 48, LGD was 38, HGD was 42, and malignancy was 123 ($p < 0.01$). The AIPP ROC curve between malignant versus non-

malignant tissue was 0.96 (0.93–0.99). An AIPP value of 60 can differentiate malignancy with 87 % sensitivity and 90 % specificity. The mean β for normal tissue was 0.490, LGD was 0.379, HGD was 0.345, and cancer was 0.453 ($p = 0.013$), with a normal tissue mean rank of 6.5 compared to 2.5 for HGD ($p = 0.029$).

Conclusions SHG signal intensity can differentiate malignant from non-malignant colonic polyp tissue with high sensitivity and specificity. Anisotropic polarization can discern HGD from normal colonic polyp tissue. SHG can thus distinguish both HGD and malignant lesions in an objective numeric fashion, without contrast agents or interpretation skills. SHG could be incorporated into endoscopy equipment to enhance white light endoscopy.

Keywords Colon cancer · Endoscopy · Second harmonic generation · Anisotropy · Imaging

J. W. Birk (✉) · M. Tadros
Division of Gastroenterology and Hepatology, University of
Connecticut Health Center, 263 Farmington Avenue,
Farmington, CT 06030-1845, USA
e-mail: birk@uchc.edu

M. Tadros
e-mail: mtadros@resident.uchc.edu

K. Moezardalan
Department of Gastroenterology, Sacramento Medical Center,
2025 Morse Avenue, Sacramento, CA 95825, USA
e-mail: kmardalan@yahoo.com

O. Nadyarnykh
Faculty of Science, Utrecht University, Postbus 80.010,
3508 TA Utrecht, The Netherlands
e-mail: o.nadyarnykh1@uu.nl

F. Forouhar
Department of Pathology and Laboratory Medicine, University
of Connecticut Health Center, 263 Farmington Avenue,
Farmington, CT 06030-3985, USA

J. Anderson
Section of Gastroenterology, Dartmouth-Hitchcock Medical
Center, One Medical Center Drive, Lebanon, NH 03756, USA

P. Campagnola
Department of Biomedical Engineering, College of Engineering,
University of Wisconsin-Madison, 1415 Engineering Drive,
Madison, WI 53706, USA

Introduction

Endoscopic examination technology has improved over the last two decades [1–3]. Advances include improved visual detection such as high-definition white light and narrow band imaging (NBI) [2], and enhanced imaging such as confocal [4] and elastography [5] try to achieve a virtual biopsy. Second harmonic generation (SHG) is a novel imaging technology that could provide for a virtual biopsy during endoscopy with advantages over confocal and other current imaging technologies [6–8].

The ability to perform accurate real-time histological-like diagnosis during routine endoscopy is a major goal in the development of new endoscopic imaging techniques [2]. The standard taxing process of histological diagnosis involves removal of tissue by mucosal biopsy or snare then retrieving and processing the tissue. Processing includes putting it into 10 % buffered formalin, paraffin embedding, staining [usually with hematoxylin and eosin (H&E)], and then, examination under standard bright-field white light microscopy. Drawbacks include cost, wait time for results, and the excisional process itself with its inherent risks of adverse events such as bleeding or perforation. Thus, development of new imaging technologies capable of detecting microscopic tumors or precursor lesions can be of tremendous help.

Over the past 20 years, numerous clinical uses for SHG have been developed [9–29]. SHG's hallmark feature is in analyzing the architecture of collagen in the extracellular matrix (ECM) [8, 30].

SHG is a coherent nonlinear process wherein two lower energy photons are upconverted to exactly twice the incident frequency (or half the wavelength) of an excitation laser [30, 31]. Like the more familiar two-photon excited fluorescence (TPEF) microscopy, SHG can provide intrinsic optical sectioning and affords enhanced imaging depths into tissues of up to 500 μ [6, 30, 32]. Due to the underlying physics of SHG's effect on tissue, a contrast mechanism is evoked which is sensitive to changes within the collagen matrix. SHG can directly visualize the collagen assembly in the ECM with no need for any exogenous staining [6, 30, 32]. ECM collagen is a very bright source of SHG image reflection [7–9, 32, 33]. SHG examination of collagen content along with some structural proteins creates very discriminating imaging [10]. SHG thus provides a potent tool for visualizing pathological effects on the ECM. For example, in animal tumor models SHG microscopy has shown that collagen adopts an abnormal structure on which transformed cells exhibit increased motility [26]. Evaluating the changes in the composition and structure of the ECM may be a promising approach as these changes are thought to be critical for tumor initiation and progression [10, 20, 34–38].

ECM changes elicit a cascade of events involving fibroblasts and tumor cells that eventually lead to a development of more aggressive tumor cells [20, 37–39]. It has recently been proposed that changes in the ECM can be used as surrogate markers for tumor invasion and therefore as a means of differentiating malignant from non-malignant tissue [10, 11, 16].

The first application of SHG for biological imaging reported in 1986 by Freund et al. [40] demonstrated the distinct polarity of collagen fibers in rat tail tendon. Since then, different experimental and clinical uses for SHG have been developed [8–14, 16, 18, 20–26, 28–30, 39, 41–43]. SHG has been used to study breast, ovarian, and skin tumors [27]. Additionally, SHG has been used to study diseases of the eye, bones, muscles, tendons, and the liver [30]. Some pilot SHG work with normal and dysplastic colonic tissues showed a possible difference in the depth-dependent signal decay; the authors hypothesized that differences could be attributed to distribution, alignment, or size of collagen fibers [44]. Zhou and his colleagues have also described using SHG to evaluate colonic crypt basement membrane shapes to evaluate for dysplasia and carcinoma [45].

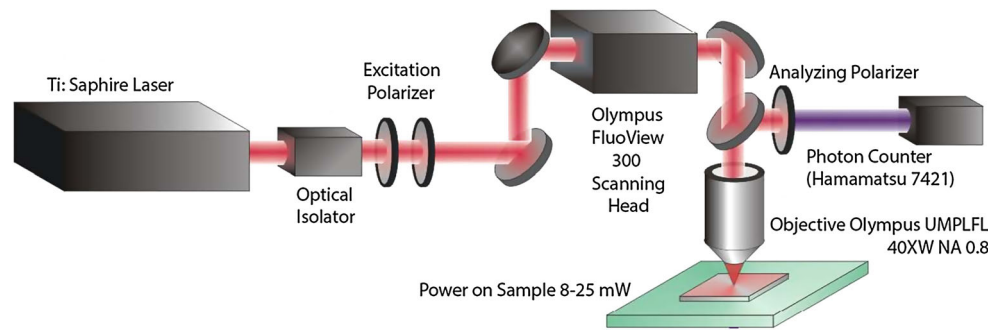
The purpose of this initial study was to evaluate the feasibility of using SHG microscopy to differentiate between malignant, dysplastic, and non-malignant human colon biopsy samples; we hypothesized that there would be a difference in the ECM structure across normal and pathological colonic tissues. In order to investigate this possibility, we used high-resolution ($\sim 0.5 \mu$) SHG imaging microscopy to objectively quantify differences in the ECM structure of normal, LGD, HGD, and malignant colon slide samples.

Methods

Study Design

Our study was approved by the University of Connecticut Health Center Institutional Review Board (IRB). A total of sixteen 500- μ -thick H&E stained slides from colon biopsies were obtained from a pool of pre-existing pathology slides located in the Department of Pathology and Laboratory Medicine of the University of Connecticut Health Center for inclusion in this study. Four slides from each of the different categories were selected: normal colonic mucosa, polyps with LGD, polyps with HGD, and malignant tumors. The study was conducted in two stages: The first was to measure SHG intensity, and the second was to evaluate the collagen fibers' alignment by calculating the anisotropy parameter β . Images were analyzed as 2D.

Fig. 1 Simplified diagrammatic illustration of the SHG microscope



TPEF and SHG Imaging System

The details of the imaging system used in this study have been well documented previously [44]. In summary, it consists of a laser scanning unit (FluoView 300; Olympus, Center Valley, PA, USA) installed on an upright microscope stand (BX61; Olympus), which is coupled to a mode-locked Titanium Sapphire femtosecond laser (Mira; Coherent, Santa Clara, CA, USA). An excitation wavelength of 890 nm with an average power of ~ 20 mW with a water immersion 40×0.8 NA objective was used to obtain all SHG imaging; this excitation wavelength was chosen to provide good depth of penetration and also to exclude most of the potentially confounding sources of two-photon excited autofluorescence, which are predominantly excited at shorter wavelengths. Our choice of wavelength and NA objective resulted in lateral and axial resolutions of approximately 0.7 and 2.5 μ , respectively. The microscope collected the reflective components of the SHG intensity using a calibrated detector (7421 GaAsP photon counting modules; Hamamatsu, Hamamatsu City, Japan). The SHG wavelength (445 nm) was isolated with a 10-nm-wide band-pass filter (Semrock, Rochester, NY, USA). Figure 1 shows a simplified illustration of the SHG microscope.

SHG Intensity Measurement

Using the imaging system described above [10, 32], both TPEF and SHG microscopy were done consecutively measuring ten randomly selected different image points from each of the 16 slides used. The random points on each slide were averaged in order to obtain a more accurate measurement for each slide. SHG reflective intensity was measured. The average intensity per pixel (AIPP) was calculated for each slide by dividing the sum of all intensities by the total number of pixels. The SHG images were analyzed using Image J software (NIH).

Anisotropy Parameter β Calculation

The anisotropy of SHG can be used to quantify collagen fiber alignment. The anisotropy parameter was calculated by:

$$\beta = (I_{\text{par}} - I_{\text{orth}}) / (I_{\text{par}} + 2 I_{\text{orth}})$$

where I_{par} and I_{orth} correspond to SHG intensity detected when the analyzing polarizer is oriented parallel and perpendicular to the laser polarization [30, 32]. Values of β range from 0 to 1, where 0 represents completely random organization of ECM fibers and one represents completely aligned organization of ECM fibers.

In our experiment, images were taken with the analyzing polarizer in the parallel and orthogonal positions. Intensities of parallel (I_{par}) and orthogonal (I_{orth}) components were measured, and the anisotropy parameter was calculated as above. Four values, one from each of the four slides, were calculated for each tissue category (normal, LGD, HGD, and cancer).

Statistical Analysis

SPSS (version 18) was used for all statistical analysis. The Kruskal–Wallis test was used to analyze nonparametric continuous variables to evaluate the difference between the mean AIPP and to compare the anisotropy parameter β of the four different groups. The area under the ROC curve was calculated for AIPP to differentiate malignant from non-malignant samples. Post hoc analysis was done using the Mann–Whitney U test to compare the anisotropy parameter β of normal tissue and HGD tissue.

Results

SHG Intensity Measurement

The mean AIPP for normal colon mucosa was 48 ± 11 , LGD was 38 ± 2 , HGD was 42 ± 13 , and malignant colon tissue was 123 ± 75 . Samples with malignancy had a significantly higher AIPP ($p < 0.01$) compared with normal, low-grade, and high-grade dysplasia samples. There was no significant difference in AIPP among other subgroups (Fig. 2; Table 1).

The area under the ROC curve (AUC) was calculated for AIPP differentiating between malignant versus non-malignant slides using pathology as the gold standard. The

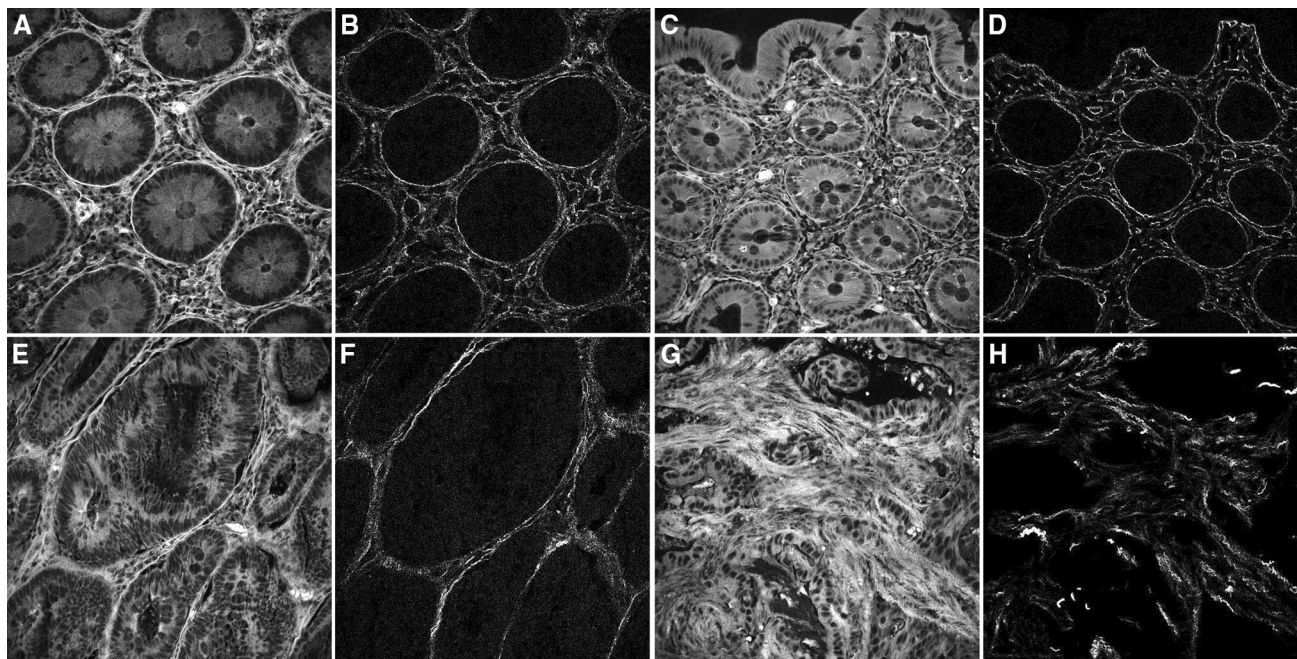


Fig. 2 TPEF and SHG microscopy images for normal, LGD, HGD, and malignancy. **a** Normal colonic mucosa (TPEF), **b** normal colonic mucosa (SHG), **c** low-grade dysplasia (TPEF), **d** low-grade dysplasia

(SHG), **e** High-grade dysplasia (TPEF), **f** high-grade dysplasia (SHG), **g** malignancy (TPEF), **h** malignancy (SHG)

Table 1 Average intensity per pixel (AIPP) in normal, low-grade dysplasia, high-grade dysplasia, and malignant samples

Sample	AIPP
Normal	48
Low-grade dysplasia	38
High-grade dysplasia	42
Malignant	123*

* $p < 0.01$

AUC was 0.96 (0.93–0.99). An AIPP threshold value of 60 was able to differentiate malignant from non-malignant with a sensitivity of 87 % and specificity of 90 % (Fig. 3).

Anisotropy Parameter β Calculation

The mean β for normal tissue was 0.490 ± 0.018 , LGD was 0.379 ± 0.053 , HGD was 0.345 ± 0.079 , and cancer was 0.453 ± 0.037 . Using the Kruskal–Wallis test, the mean rank for normal was calculated to be 14, LGD was 5.75, HGD was 4, and cancer was 10.25. The difference was statistically significant $p = 0.013$ (Table 2). Post hoc analysis was done and normal tissue had a mean rank of 6.5 compared to 2.5 for HGD. This was also statistically significant ($p = 0.029$). HGD had the lowest β , indicating the highest proportion of non-aligned fibers (Table 3).

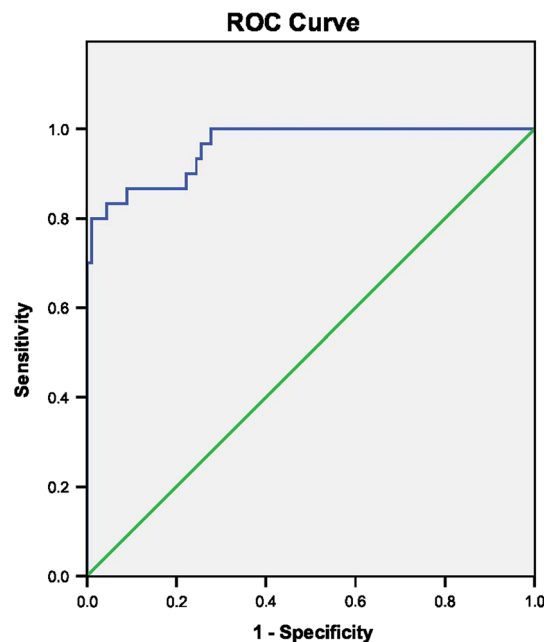


Fig. 3 ROC curve for AIPP to differentiate malignant from non-malignant polyps

Discussion

There are multiple optical advantages of SHG. One not evaluated here is SHG intrinsic 3D dimensionality. SHG, like TPEF, has the ability for optical sample sectioning,

Table 2 Kruskal–Wallis mean rank for anisotropy parameter β for normal, low-grade dysplasia, high-grade dysplasia, and malignant tissues

Sample	Mean β	Mean rank order
Normal	0.49	14
LGD	0.379	5.75
HGD	0.345*	4**
CA	0.453	10.25

* $p = 0.013$; ** $p = 0.029$

Table 3 Post hoc analysis of anisotropy parameter β between normal and high-grade dysplasia polyps

Sample	N	Mean ranks
Normal	4	6.5
HGD	4	2.5*

* $p = 0.029$

yet, unlike TPEF, the image is sharper because it does not involve fluorescence imaging. The SHG laser wavelength is in the near infrared spectral range (700–1,000 nm), and therefore, it can achieve high penetration while maintaining good resolution. Furthermore, SHG images tissues in situ, without the need for preparation like histology and potentially tissue damaging exogenous contrast labels like chromoendoscopy and confocal endoscopy. SHG has substantially less bleaching effects relative to other fluorescence methods, as the SHG reflective signals arise from an induced polarization rather than from only absorption [18, 30]. Also, in auto fluorescence, the reflective contrast is not distinct and hence cannot be used for anisotropy measurements.

The application of SHG to diagnose changes in the ECM in tumors compared with normal tissue has been utilized in the past. SHG has been shown to elucidate changes in both collagen content [30] and arrangement [28] in both ovarian and breast cancer [10, 11, 20, 39]. Others have applied SHG collagen assembly in evaluating the limits of skin tumor borders [10, 11].

Our work demonstrated the utility of SHG in both signal intensity and alignment of collagen content and showed a significantly higher SHG intensity in the malignant samples reflecting higher collagen content; this could be used as a diagnostic tool to differentiate malignant from non-malignant samples. Results showed normal tissue having the highest anisotropy β value, which denotes the most aligned collagen fibers, while HGD had the lowest β value, denoting the most misaligned collagen fibers. This could signify that SHG can recognize early changes in the ECM of HGD, before its progression to invasive cancer, with a more orderly collagen fiber deposition better suited for frank

invasion of surrounding tissue. The ability of SHG anisotropic polarization to detect early changes in HGD gives SHG a unique utility, since using signal intensity alone has inherent weaknesses in specificity. By combining both SHG intensity and the β anisotropy parameter, we can distinguish both high-grade dysplastic and malignant lesions from normal tissues. The ability of SHG to make such distinction has several obvious advantages. It does not need interpretation experience or dye as required with confocal techniques [4, 5], and it provides numeric values for both AIPP and β anisotropy, which are more objective. Additionally, SHG uses a fixed intensity femtosecond-pulsed beam, instead of a continuous one as used in the confocal endoscopies, making it less likely to cause heat or other toxic injury to tissue. SHG could easily be incorporated into endoscopy equipment, in a similar fashion to NBI and Fuji Intelligent Chromo Endoscopy (FICE) to enhance endoscopy and can potentially be used in imaging during live endoscopy to diagnose HGD and malignant lesions. With miniaturization and integration into endoscopy equipment, SHG has the potential to provide real time “optical biopsy” during colonoscopy or endoscopy. As this is an early study on SHG practicality, further studies will need to be performed to verify findings of fresh unstained polyps and “in vivo” on patients during colonoscopy to elucidate the true future role of SHG in gastroenterological endoscopic imaging.

Acknowledgments The authors thank Ms. Amy Pallotti (UConn Health Center) for her assistance with formatting and submitting the article.

Conflict of interest None.

References

1. Brkic T, Kalauz M, Ostojic R. Novel endoscopic optical techniques for the detection of early gastrointestinal neoplasia. *Lijec Vjesn.* 2009;131:69–73.
2. Monkemuller K, Neumann H, Fry LC. Enteroscopy: advances in diagnostic imaging. *Best Pract Res Clin Gastroenterol.* 2012;26: 221–233.
3. Aisenberg J. Gastrointestinal endoscopy nears “the molecular era”. *Gastrointest Endosc.* 2008;68:528–530.
4. ASGE Technology Committee, Kantsevoy SV, Adler DG, et al. Confocal laser endomicroscopy. *Gastrointest Endosc.* 2009;70: 197–200.
5. Saftoiu A, Vilman P. Endoscopic ultrasound elastography—a new imaging technique for the visualization of tissue elasticity distribution. *J Gastrointest Liver Dis.* 2006;15:161–165.
6. Campagnola PJ, Millard AC, Terasaki M, Hoppe PE, Malone CJ, Mohler WA. Three-dimensional high-resolution second-harmonic generation imaging of endogenous structural proteins in biological tissues. *Biophys J.* 2002;82:493–508.
7. Wang M, Reiser KM, Knoesen A. Spectral moment invariant analysis of disorder in polarization-modulated second-harmonic-generation images obtained from collagen assemblies. *J Opt Soc Am A Opt Image Sci Vis.* 2007;24:3573–3586.

8. Cox G, Kable E, Jones A, Fraser I, Manconi F, Gorrell MD. 3-dimensional imaging of collagen using second harmonic generation. *J Struct Biol.* 2003;141:53–62.
9. Han M, Giese G, Bille JF. Second harmonic generation imaging of collagen fibrils in cornea and sciera. *Opt Express.* 2005;13: 5791–5797.
10. Nadiarnykh O, LaComb RB, Brewer MA, Campagnola PJ. Alterations of the extracellular matrix in ovarian cancer studied by second harmonic generation imaging microscopy. *BMC Cancer.* 2010;10:94.
11. Ajeti V, Nadiarnykh O, Ponik SM, Keely PJ, Eliceiri KW, Campagnola PJ. Structural changes in mixed col I/Col V collagen gels probed by SHG microscopy: implications for probing stromal alterations in human breast cancer. *Biomed Opt Express.* 2011;2:2307–2316.
12. Débarre D, Supatto W, Pena A, et al. Imaging lipid bodies in cells and tissues using third-harmonic generation microscopy. *Nat Methods.* 2006;3:47–53.
13. Deniset-Besseau A, Dubois J, Benkhou E, Hache F, Brevet P, Schanne-Klein M. Measurement of the second-order hyperpolarizability of the collagen triple helix and determination of its physical origin. *J Phys Chem B.* 2009;113:13437–13445.
14. Han M, Zickler L, Giese G, Walter M, Loesel FH, Bille JF. Second-harmonic imaging of cornea after intrastromal femto-second laser ablation. *J Biomed Opt.* 2004;9:760–766.
15. Lacombe R, Nadiarnykh O, Campagnola PJ. Quantitative SHG imaging of the diseased state osteogenesis imperfecta: experiment and simulation. *Biophys J.* 2008;94:4104.
16. Lin S, Jee S, Kuo C, et al. Discrimination of basal cell carcinoma from normal dermal stroma by quantitative multiphoton imaging. *Opt Lett.* 2006;31:2756–2758.
17. Matteini P, Ratto F, Rossi F, et al. Photothermally-induced disordered patterns of corneal collagen revealed by SHG imaging. *Opt Express.* 2009;17:4868–4878.
18. Nadiarnykh O, Plotnikov S, Mohler WA, Kalajzic I, Redford-Badwal D, Campagnola PJ. Second harmonic generation imaging microscopy studies of osteogenesis imperfecta. *J Biomed Opt.* 2007;12:051805.
19. Plotnikov S, Juneja V, Isaacson AB, Mohler WA, Campagnola PJ. Optical clearing for improved contrast in second harmonic generation imaging of skeletal muscle. *Biophys J.* 2006;90: 328–339.
20. Provenzano PP, Eliceiri KW, Campbell JM, Inman DR, White JG, Keely PJ. Collagen reorganization at the tumor-stromal interface facilitates local invasion. *BMC Med.* 2006;4:38.
21. Strupler M, Pena A, Hernest M, et al. Second harmonic imaging and scoring of collagen in fibrotic tissues. *Opt Express.* 2007;15: 4054–4065.
22. Sun W, Chang S, Tai DCS, et al. Nonlinear optical microscopy: use of second harmonic generation and two-photon microscopy for automated quantitative liver fibrosis studies. *J Biomed Opt.* 2008;13:064010.
23. Tai S, Tsai T, Lee W, et al. Optical biopsy of fixed human skin with backward-collected optical harmonics signals. *Opt Express.* 2005;13:8231–8242.
24. Tan H-, Sun Y, Lo W, et al. Multiphoton fluorescence and second harmonic generation imaging of the structural alterations in keratoconus ex vivo. *Invest Ophthalmol Vis Sci.* 2006;47:5251–5259.
25. Theodossiou TA, Thrasivoulou C, Ekwoji C, Becker DL. Second harmonic generation confocal microscopy of collagen type I from rat tendon cryosections. *Biophys J.* 2006;91:4665–4677.
26. Williams RM, Zipfel WR, Webb WW. Interpreting second-harmonic generation images of collagen I fibrils. *Biophys J.* 2005;88:1377–1386.
27. Yeh AT, Choi B, Nelson JS, Tromberg BJ. Reversible dissociation of collagen in tissues. *J Invest Dermatol.* 2003;121:1332–1335.
28. Brown E, McKee T, diTomaso E, et al. Dynamic imaging of collagen and its modulation in tumors in vivo using second-harmonic generation. *Nat Med.* 2003;9:796–800.
29. Cicchi R, Massi D, Sestini S, et al. Multidimensional non-linear laser imaging of basal cell carcinoma. *Opt Express.* 2007;15: 10135–10148.
30. Campagnola P. Second harmonic generation imaging microscopy: applications to diseases diagnostics. *Anal Chem.* 2011;83: 3224–3231.
31. Shen Y. *The Principles of Nonlinear Optics.* New York: Wiley-Interscience; 1984.
32. Campagnola PJ, Loew LM. Second-harmonic imaging microscopy for visualizing biomolecular arrays in cells, tissues and organisms. *Nat Biotechnol.* 2003;21:1356–1360.
33. Odin C, Le Grand Y, Renault A, Gailhouste L, Baffet G. Orientation fields of nonlinear biological fibrils by second harmonic generation microscopy. *J Microsc.* 2008;229:32–38.
34. Ricciardelli C, Rodgers RJ. Extracellular matrix of ovarian tumors. *Semin Reprod Med.* 2006;24:270–282.
35. Pupa SM, Menard S, Forti S, Tagliabue E. New insights into the role of extracellular matrix during tumor onset and progression. *J Cell Physiol.* 2002;192:259–267.
36. Theret N, Musso O, Turlin B, et al. Increased extracellular matrix remodeling is associated with tumor progression in human hepatocellular carcinomas. *Hepatology.* 2001;34:82–88.
37. Huang S, Van Arsdall M, Tedjarati S, et al. Contributions of stromal metalloproteinase-9 to angiogenesis and growth of human ovarian carcinoma in mice. *J Natl Cancer Inst.* 2002;94: 1134–1142.
38. Hugo H, Ackland ML, Blick T, et al. Epithelial–mesenchymal and mesenchymal–epithelial transitions in carcinoma progression. *J Cell Physiol.* 2007;213:374–383.
39. Provenzano PP, Inman DR, Eliceiri KW, et al. Collagen density promotes mammary tumor initiation and progression. *BMC Med.* 2008;6:11.
40. Freund I, Deutsch M, Sprecher A. Connective tissue polarity. Optical second-harmonic microscopy, crossed-beam summation, and small-angle scattering in rat-tail tendon. *Biophys J.* 1986; 50:693–712.
41. Cicchi R, Kapsokalyvas D, De Giorgi V, et al. Scoring of collagen organization in healthy and diseased human dermis by multiphoton microscopy. *J Biophotonics.* 2010;3:34–43.
42. LaComb R, Nadiarnykh O, Townsend SS, Campagnola PJ. Phase matching considerations in second harmonic generation from tissues: effects on emission directionality, conversion efficiency and observed morphology. *Opt Commun.* 2008;281:1823–1832.
43. Plotnikov SV, Millard AC, Campagnola PJ, Mohler WA. Characterization of the myosin-based source for second-harmonic generation from muscle sarcomeres. *Biophys J.* 2006;90:693–703.
44. Zhuo S, Zhu X, Wu G, Chen J, Xie S. Quantitative biomarkers of colonic dysplasia based on intrinsic second-harmonic generation signal. *J Biomed Opt.* 2011;16:120501.
45. Zhuo S, Yan J, Chen G, et al. Label-free imaging of basement membranes differentiates normal, precancerous, and cancerous colonic tissues by second-harmonic generation microscopy. *PLoS One.* 2012;7:e38655.